RESEARCH ARTICLE

Macromolecular Materials and Engineering
www.mame-journal.de

Glycerol-Based Polyurethane Nanoparticles Reduce Friction and Wear of Lubricant Formulations

Fabian Uebel, Héloïse Thérien-Aubin, and Katharina Landfester*

The relative motion of two surfaces in direct contact results in friction and wear. This affects every moving surface, contributing to a quarter of the worldwide energy consumption. The addition of lubricant can reduce friction by separating the surfaces, making more energy-efficient systems. Lubricants are composed of a base oil and a series of additives. Molecules like glycerol can improve the efficiency of a lubricant system. However, the direct addition of hydrophilic molecules to hydrophobic lubricant oils is challenging due to their poor miscibility. The encapsulation of glycerol, or other hydrophilic additives, in nanocarriers will enable the design of additive systems delivering poorly miscible molecules to the lubricant. Here, glycerol is encapsulated in cross-linked glycerol nanocapsules. The nanocarrier is dispersed in a lubricant oil and placed between two metal surfaces. The release of the additive, from the nanocarriers, is triggered by the force applied on the nanocarriers by the metal surfaces in contact. The release observed is dependent on the applied force and mechanical properties of the nanocarrier, which can be controlled during the synthesis. The addition of those mechanoresponsive nanocarriers improved the long-term performance of the lubricant and represents a step toward the reduction of friction between metal–metal contacts.

1. Introduction

The energy consumption of our modern society is immense, and we require actions to deal with the increasingly severe energy crisis we are facing today.[1] Friction and wear between moving surfaces contribute to 23% of the total worldwide energy consumption.[2] Most of this energy (20%) is consumed to overcome friction, and 3% is associated with wear-related failures. Consequently, developing new surfaces, materials, or additives to reduce friction and wear would significantly impact our energy consumption.

Two interacting surfaces in relative motion create a tribological pair. The friction, the force resisting the movement, of the tribological pair can be partially ascribed to the direct contact of the surfaces, which the presence of microscopic roughness can enhance. The addition of a lubricant creates a lubricating film in the tribological system, which can separate the two interacting surfaces. This reduces the friction and makes the tribological contact more energy efficient.

Depending on the load applied at the contact, the sliding speed of the surfaces, and the viscosity of the lubricant, different lubrication regimes can be reached (boundary, mixed, and hydrodynamic).[3,4] While direct contact between the surfaces occurs in boundary lubrication, only limited contacts between asperities are observed in the mixed regime, and the surfaces are fully separated by a lubricating film in the hydrodynamic lubrication regime. The minimization of hydrodynamic shear is one of the key approaches to optimizing a lubricant system by tuning its rheological properties. This often means decreasing the lubricant viscosity to the lowest possible value, while maintaining the tribological system in a mixed or hydrodynamic lubrication regime to minimize direct contact between the surfaces. Another approach in reducing the friction in tribological contacts consists in the addition of friction modifiers in low concentrations. Compounds such as organo–molybdenum complexes, functionalized polymers, nanoparticles, or amphiphilic organic molecules are widely used as friction modifiers.[5] Typically, the addition of friction modifiers leads to the formation of a monolayer at the surface–oil interface due to their amphiphilic character.[6] The addition of this layer of friction-modifying molecules can reduce shear forces by interacting with the nonpolar oil and the polar metal surface simultaneously. In most lubricant systems, both friction modifiers and viscosity modifiers are used simultaneously.

One of the Achilles' heels of lubricant systems is their deterioration over time during their service. This leads to immense economic and environmental costs by creating the need to replace the lubricant system frequently. In addition to friction modifiers, other additives are used to extend the life of the lubricant system, such as antioxidants, corrosion inhibitors, antiwear and

F. Uebel, H. Thérien-Aubin, K. Landfester
Max Planck Institute for Polymer Research
Ackermannweg 10, Mainz 55128, Germany
E-mail: htherienaubin@mun.ca
H. Thérien-Aubin
Department of Chemistry
Memorial University of Newfoundland
283 Prince Philip Dr, St. John's, NL A1B 3X7, Canada

The ORCID identification number(s) for the author(s) of this article can be found under https://doi.org/10.1002/mame.202100821

DOI: 10.1002/mame.202100821

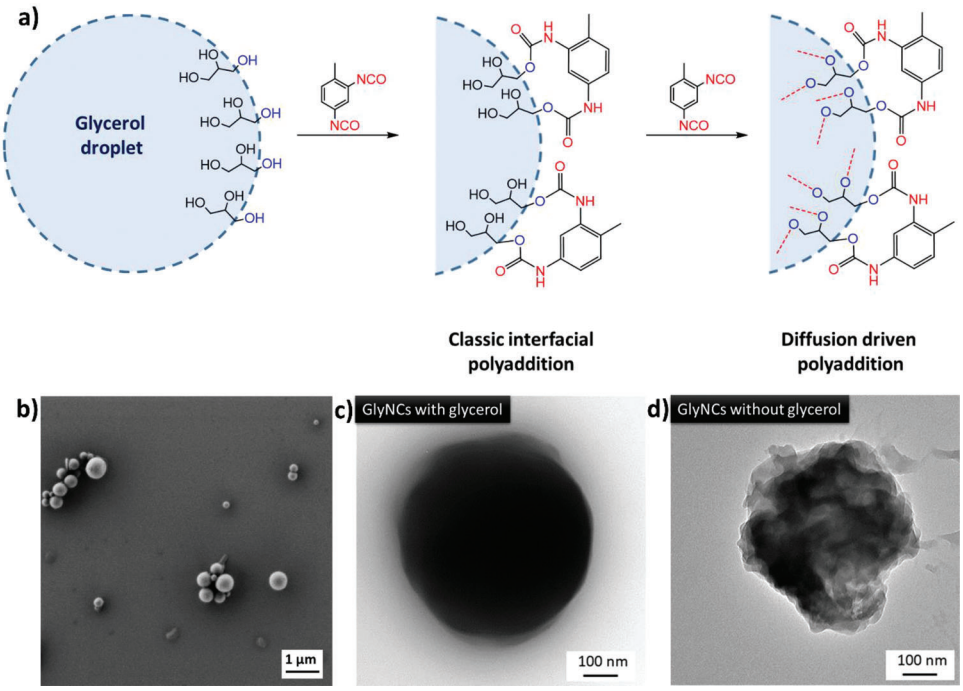

Figure 1. Synthesis of GlyNCs. a) Polyaddition reaction of glycerol droplets and 2,4-toluene diisocyanate. b) SEM images of GlyNCs. TEM image of GlyNC c) before the removal of the encapsulated free glycerol and d) after removal of the unreacted glycerol.

antifoam agents, or viscosity index improvers.[7] The addition of a new component to the lubricant oil is often limited by miscibility. For example, glycerol adheres to metal surface and creates a new interface of solid surface/glycerol film/lubricant oil, which allows for the reduction of shear forces by generating a new low-shear-strength glycerol film.[8,9] However, the addition of glycerol to nonpolar hydrophobic lubricant oils is not possible due to the poor miscibility of glycerol in most base oil used industrially. Therefore, glycerol is either used in aqueous lubricants[10] or as derivatives, such as glycerol monooleate, in hydrophobic lubricant oils. However, the friction-reducing effect of glycerol derivatives is limited, compared to pure glycerol.[8,11] Consequently, the delivery of glycerol and other hydrophilic friction-modifying agents to a hydrophobic oil could significantly reduce the friction in a lubricated system by forming a film at the surface of the metal contact. In order to introduce enough glycerol in hydrophobic-based oils, new delivery mechanisms need to be developed, like the encapsulation of hydrophilic compounds in responsive nanocapsules to circumvent their poor miscibility.

Nanoparticles are a new class of lubricant additives.[12–14] Their size allows them to enter the contact region between the lubricated surfaces.[15] At the contact, nanoparticles can influence the lubrication either through rolling, sliding, or exfoliation, depending on the contact pressure at the tribological contact and the nanoparticle morphology.[16] In comparison with organic additives, many nanoparticle additives are thermally more stable and can operate at elevated temperatures, extending the range of temperature at which the lubricant systems can be used.[17] Combining the intrinsic friction-reducing properties of nanoparticles with the ability to encapsulate and release additional friction-modifying molecules inside the nanoparticles will lead to the development of a novel class of lubricant additives able to control and extend the life cycle of the lubricant.

Mechanoresponsive release is an ideal approach to design smart additives for lubrication. Release triggered by a mechanoresponsive mechanism triggered could occur under the influence of external forces on a nanocarrier[18] and can be harnessed to release friction modifiers when the forces present in a tribological contact exceed a predetermined threshold. This approach will lead to the design of self-regulating systems, where increasing forces, for example, due to the lubricant depletion, induce the release of fresh lubricating molecules from the nanocarriers, restoring the original low-friction properties.

Here, we establish the synthesis and characterization of mechanoresponsive nanocarrier additives able to release glycerol. First, the partial polymerization of glycerol with a crosslinking agent yielded glycerol-based nanoparticles composed of a solid polyurethane network surrounding unreacted free glycerol. These nanocarriers were compatible with traditional hydrophobic lubricant systems based on poly(α-olefin) (PAO) and displayed a strong friction-modifying effect in steel–steel contacts. This type of nanocarrier is an elegant approach to deliver hydrophilic additives, like glycerol, in hydrophobic lubricant systems, resulting in the control of the tribological properties in a metal–metal contact.

2. Results and Discussion

Figure 1 shows the synthesis of the glycerol nanocarriers (GlyNCs). First, a miniemulsion of nanometer-sized glycerol nanodroplets in toluene, stabilized by the presence of polyglycerol polyricinoleate (PGPR) used as a surfactant, was prepared by microfluidization (Figure S1, Supporting Information).[19] Then,

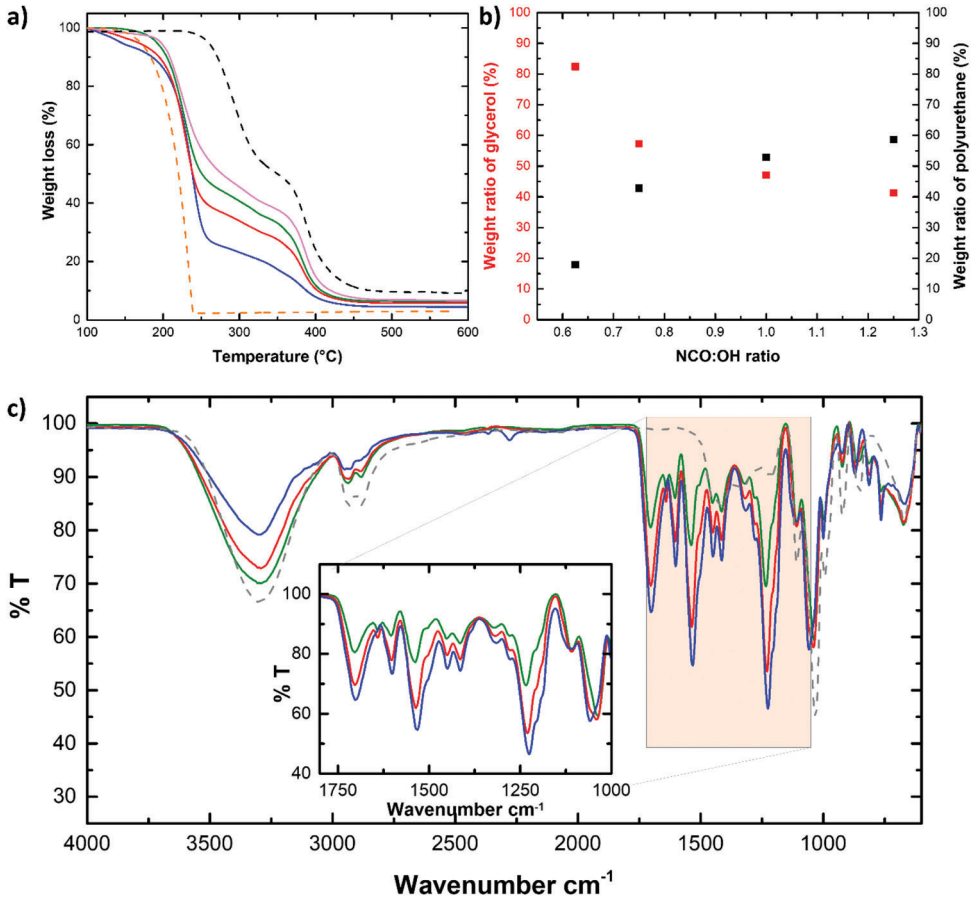

Figure 2. a) TGA decomposition analysis of GlyNCs with different NCO:OH (blue: 0.625; red: 0.75; green: 1.0; magenta: 1.25), pure glycerol (orange dashes), and glycerol-free GlyNCs (black dashes). b) Weight ratio of unreacted glycerol and formed polyurethane network of GlyNCs with different cross-linking ratios. c) FTIR spectra of GlyNCs with different NCO:OH ratio (blue: 0.64; red: 0.32; green: 0.16; grey dots: pure glycerol). Inset showing the formed polyurethane linkages from 1150 to 1750 cm^{-1}.

a toluene soluble cross-linking agent, toluene diisocyanate (TDI), was added to the continuous phase. Then, at the interface of the glycerol droplets and the continuous toluene phase, a polyaddition reaction between the alcohol groups of the glycerol and the isocyanate groups of the TDI led to the formation of a polyurethane network. Only a fraction of the glycerol reacted and the cross-linked polyurethane network formed at the interface trapped the unreacted glycerol molecules, as observed with other alcohol-containing systems.[20,21] The reaction led to the formation of spherical nanoparticles (Figure 1) and even though a large fraction of the glycerol remained unreacted (**Figure 2** and Figure S2, Supporting Information), the formation of a core–shell structure, observed in other systems, was not observed here. The interfacial polymerization of precursor nanodroplets can yield different conformations of nanocarriers. Here, the morphology of the GlyNCs was studied by transmission electron microscopy (TEM). Figure 1c shows that the as-prepared GlyNCs appeared as spherical nanoparticles. However, due to the lack of contrast between unreacted glycerol and the glycerol-based polyurethane network, the efficient differentiation between the carrier material (polyurethane network) and the payload (unreacted glycerol) was challenging. The transfer of the GlyNCs to water allowed the removal of unreacted glycerol, leaving only the polyurethane network. The TEM of the washed GlyNCs showed that the polyurethane network had a sponge-like morphology (Figure 1d). This morphology was likely obtained because of the existence of no (or limited) phase separation between the polyurethane network and the unreacted glycerol during the interfacial polymerization and the partial miscibility of TDI in glycerol.

Controlling the amount of cross-linker, more specifically the ratio of isocyanate groups (NCO) to hydroxyl groups (OH), yielded GlyNCs with different compositions. The variation of the NCO:OH ratio from 0.625 to 1.25 resulted in an increase in the formation of the polyurethane network as determined by TGA analysis (Figure 2a), FTIR spectroscopy (Figure 2c), and NMR spectroscopy (Figure S2, Supporting Information). The TGA curve showed a two-step degradation process for the GlyNCs containing free glycerol. The first degradation at ≈225 °C corresponded to the degradation of free glycerol, and the second degradation, starting at ≈375 °C, to the degradation of the polyurethane network. The relative weight loss of each degradation steps was used to determine the composition of GlyNCs with different NCO:OH ratios (Figure 2b). The GlyNCs were further analyzed by FTIR (Figure 2c) and NMR spectroscopy (Figure S2, Supporting Information). The formation of the urethane linkages during

the polymerization led to the apparition of new vibration mode at 1702 (C═O), 1532 (C–N), and 1228 cm^{-1} (O–C═O) (Figure 2c, inset). As the NCO:OH ratio increased, the number of urethane linkages increased, leading to an increase in the intensity of the IR peaks associated with the urethane. Simultaneously, the peak associated with the vibration of the alcohol groups (≈3300 cm^{-1}) decreased.

In turn, the composition of the GlyNCs influenced the mechanical properties of the nanocapsule. Atomic force microscopy (AFM) was used to measure the Young's modulus of GlyNCs with varying NCO:OH ratio **(Figure 3)**. After casting a dilute suspension of GlyNCs on a glass slide, individual and isolated GlyNCs were imaged by AFM (Figure 3a) in quantitative imaging mode. Quantitative imaging mode allowed recording a force–displacement curve at each pixel of the image, which was used to calculate the Young's modulus of the GlyNCs by imaging a defined section of the GlyNC. Each GlyNC displayed a narrow Gaussian distribution of Young's modulus (Figure 3b). The modulus of the GlyNCs increased from 231 to 851 MPa, when the ratio of NCO:OH increased from 0.625 to 1.25. Therefore, controlling the amount of cross-linker used during the synthesis allowed to modulate the Young's modulus of the resulting polyurethane network, and thus tune the mechanical properties and behavior of the GlyNCs.

After the synthesis, the GlyNCs (initially dispersed in toluene) were redispersed in PAO2, and the GlyNCs fully preserved their colloidal stability and remained fully dispersed (Figure S1b, Supporting Information) after the solvent transfer. This colloidal stability, provided by the presence of PGPR at the oil/nanoparticle interface, prevented the settling of the GlyNCs despite the higher density of glycerol in comparison to PAO2, at least on a time scale of several days. However, the GlyNCs can be removed from the PAO either by filtration using a membrane with pores smaller than the GlyNCs or by 20 min of centrifugation at a speed generating a centripetal force of more than 5000 × *g*.

Then, we studied the influence of the addition of GlyNCs to PAO2 on the tribological properties of a steel–steel contact in a ball-on-three-plates geometry (**Figure 4**a). During the tribological measurement, the steel ball was pressed on three steel plates with a known axial force *F*, and Stribeck curves (Figure S3a, Supporting Information) were recorded by cycling the rotation speed between 0 and 135 mm s^{-1}. To ensure the acquisition of reproducible results, the steel plates used in the experiment were first polished to remove any pre-existing irregularities (Figure S4, Supporting Information). When ramping up the sliding speed from 0 to 135 mm s^{-1}, the coefficient of friction (CoF) was recorded across different lubrication regimes (boundary-, mixed- and hydrodynamic-lubrication), as defined by Stribeck.[4] After the experiment, the wear scars on the steel plate surfaces were analyzed (Figure 4b,c).[14] Figure 4d shows how the wear scars observed after the tribological experiments were influenced by the composition of the GlyNCs used as the additive in PAO2. Typically, the wear track depth, measured by optical topography, varied between 1 and 6 μm depending on the lubricant system used. In all cases, the area of the observed wear scars reduced significantly after the addition of the GlyNCs to PAO2. Furthermore, the effect of the GlyNCs was influenced by the chemical composition. The maximal reduction in wear occurred for the suspension of GlyNCs in PAO2 with the GlyNCs prepared at an NCO:OH ra-

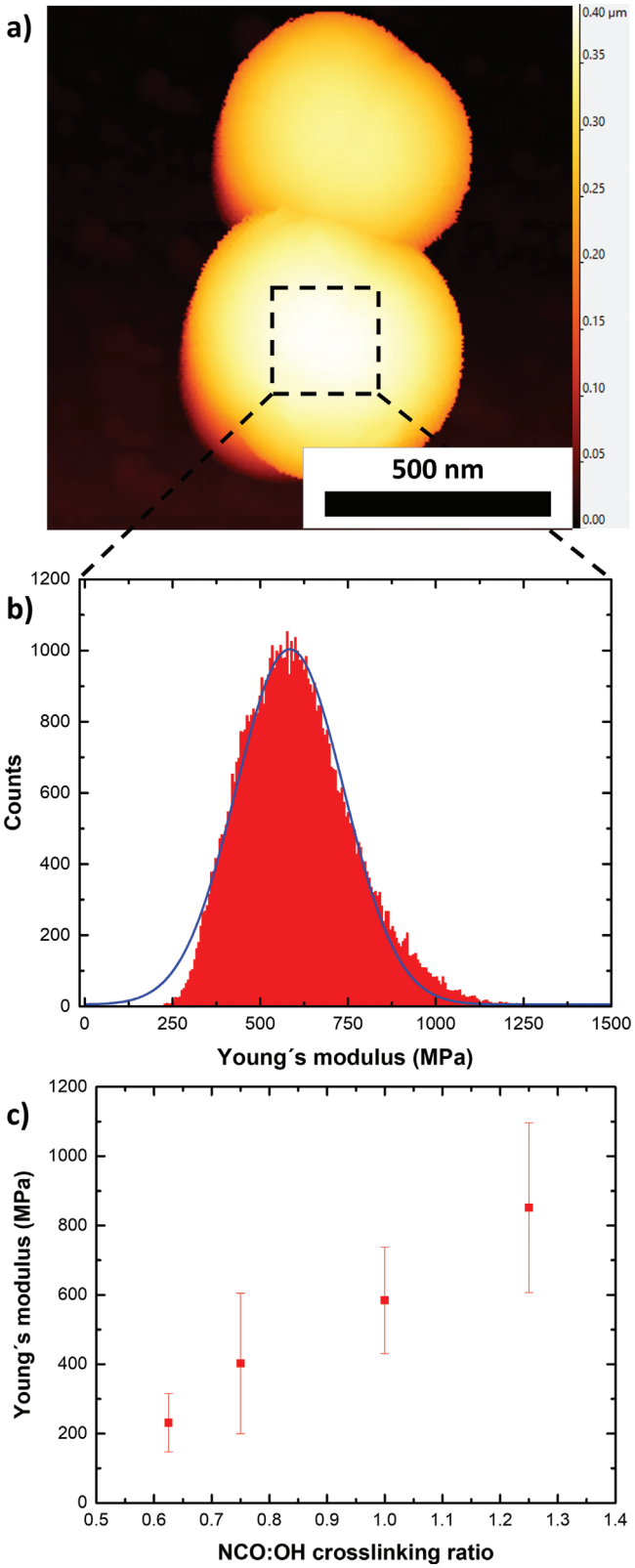

Figure 3. AFM studies of GlyNCs. a) AFM image of individual GlyNCs on a glass slide. b) Young´s modulus of a GlyNC recorded on the marked area close the pole of the nanocarrier. c) Young´s modulus of GlyNCs with different NCO:OH cross-linking ratios.

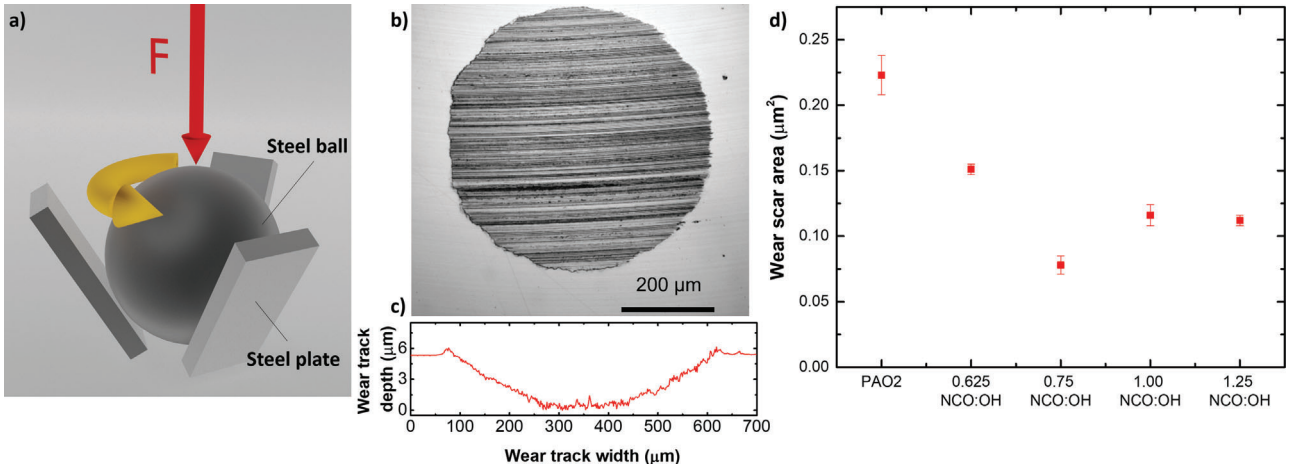

Figure 4. Tribological testing. a) Ball-on-three-plates geometry used for tribological measurements. b) Wear scar on a stainless steel plate as the result of a tribological measurement of pure PAO2 at 5 N over 25 cycles. c) Wear track profile of the wear scar from (b). d) Wear scar areas obtained after 25 cycles at 5 N axial force for mixtures of just PAO2 and GlyNCs of different NCO:OH ratios in PAO at 5 wt% loading.

tio of 0.75, indicating a dual effect of the lubrication caused by the presence of spherical nano-objects in the suspension and the release of glycerol in the tribological contact.

In addition to reducing wear at the tribological contact, the GlyNCs also influenced the CoF in the system. Therefore, we studied the friction-reducing properties of GlyNCs in PAO2 at different axial forces from 1 to 15 N, to see the effect of load on the lubrication (**Figure 5**a). The lowest CoF was observed for the highest applied load of 15 N, while a significant reduction of the CoF was already observed for 5 N. In comparison, the results obtained for pure PAO2, at the same axial loads and number of Stribeck cycle, showed higher friction.

Additionally, the effect of the concentration of GlyNC on the tribological properties of the lubricant system was analyzed (Figure 5b). As the concentration of nanoparticles in suspension increased, the viscosity of the oil increased,[22] which could have a negative effect on the lubrication of the tribological contact. While the CoF decreased minimally with the addition of 1 wt% of GlyNCs in PAO2 in comparison to pure PAO2, the CoF drastically decreased with the addition of 5 wt% of GlyNCs, and was moderately lower for the PAO2 containing 15 wt% of GlyNCs. This reduction in friction clearly shows the outstanding ability of GlyNCs as friction-reducing additives in lubricant oils.

The effect of the GlyNCs on the lubrication of the metal/metal contact was also influenced by the cross-linking degree of the GlyNCs. GlyNCs prepared with varying NCO:OH ratio were redispersed in PAO2 at a concentration of 5 wt%, and the effect of those lubricant systems on the friction in the ball-and-three-plate contact was analyzed at different axial forces (Figure 5c). Independently from the cross-linking ratio, higher axial loads always showed lower CoF than pure PAO2 under the same conditions, with the 0.75 NCO:OH ratio displaying the lowest CoF. The GlyNCs with this cross-linking ratio also showed the strongest wear-reducing effect (Figure 4d). Interestingly, the 1.0 NCO:OH ratio resulted in very similar friction for all axial loads used, and led to the strongest reduction in CoF when small loads were applied (1 and 5 N) in comparison to the GlyNCs prepared with other cross-linking ratios.

XPS measurements were performed on the surface of the steel plates after the tribological measurements. The XPS spectrum recorded inside the wear scar area showed the presence of aromatic C–C (284.8 eV), C–O (286.4 eV), O–C=O (289.1 eV), and C–N (285.6 eV) linkages, while outside the wear scar area no C–N linkages were found (**Figure 6**a). This clearly indicates that the GlyNCs, cross-linked with aromatic TDI, have entered the tribological contact during the tribological measurement.

The release of free glycerol from GlyNCs was quantified using HPLC. After the tribological measurement, the entire suspension of GlyNCs in PAO2 was collected. The samples analyzed here were collected after performing 25 Stribeck cycles. After separating the GlyNCs from PAO2 by filtration, the released glycerol was extracted from PAO2 with an acetonitrile–water mixture. This mixture was analyzed by HPLC to quantify the amount of released glycerol from the GlyNCs. The results obtained were compared to a calibration curve prepared by dissolving known amounts of glycerol in the acetonitrile–water mixture (Figure S5, Supporting Information). GlyNCs used as additive can potentially affect the friction in a tribological contact in two manners: By the friction-reducing properties of the nanocarrier itself and by the release of encapsulated glycerol, which would adhere to the polar metal surface. The application of external loads at the tribological contact can promote the mechanoresponsive release from the GlyNCs and thus a reduction of friction is expected. As Figure 6b shows, the amount of released glycerol increased with increasing axial loads applied in the tribological contact. Therefore, the lower friction observed for higher loads compared to smaller loads (Figure 5a,c) originates from the presence of more glycerol released from the GlyNCs. Although the fraction of glycerol released is comparable for all tested axial loads, lower CoFs were measured at higher axial load. Therefore, the lubricating effect observed with the GlyNCs at higher load can be attributed to both the presence of the nanoparticles themselves, and the release of glycerol. The slow and limited release of glycerol from the GlyNCs observed after 25 Stribeck cycles underlines the potential of GlyNCs as lubricant additives to improve the long-term performance of the base oil.

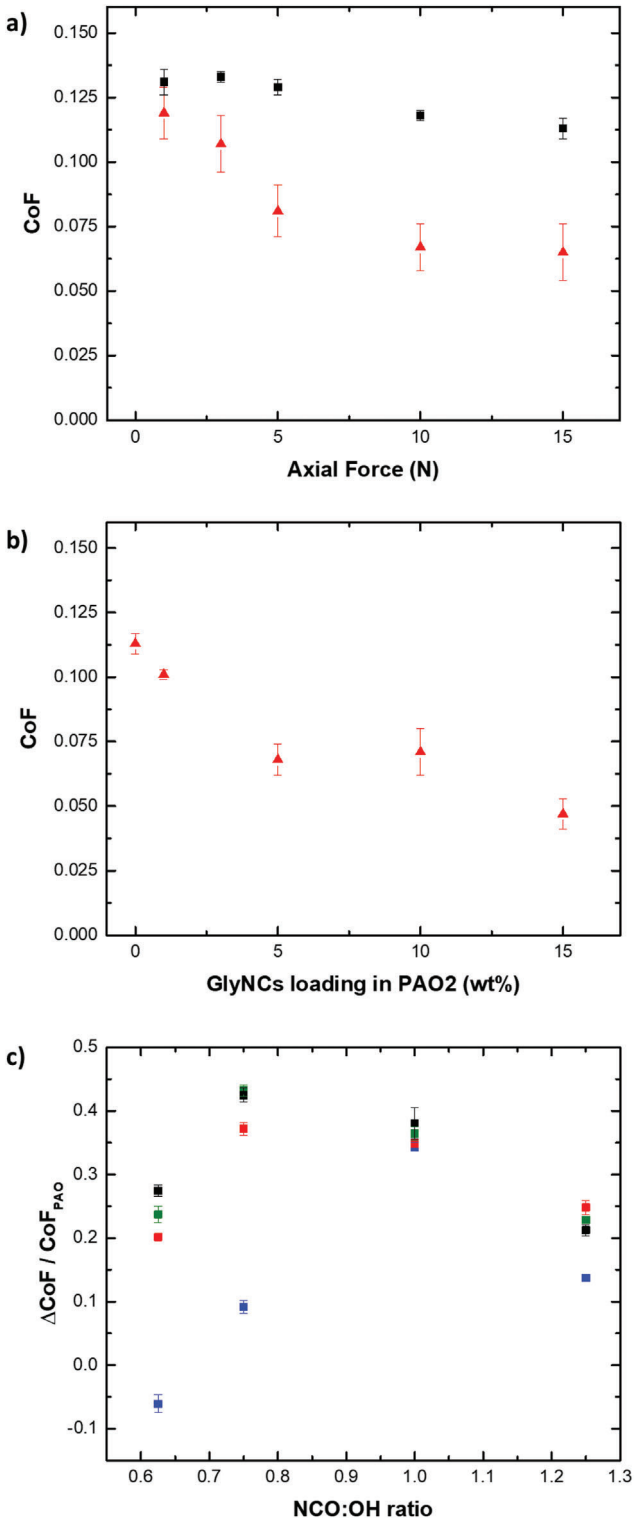

Figure 5. Tribological measurements. a) Coefficient of friction for pure PAO (black squares) and 5 wt% GlyNCs of 0.75 = NCO:OH (red triangles) measured at different axial forces. b) Coefficient of friction of GlyNCs (0.75 = NCO:OH) with different concentration in PAO2 measured at 15 N axial force. c) Relative coefficient of friction of GlyNCs with different NCO:OH cross-linking ratio in PAO2 at 5 wt% loading and at different axial forces (blue: 1 N; red: 5 N; green: 10 N; black: 15 N).

3. Conclusion

We demonstrated the synthesis of glycerol-based nanocarriers by the reaction between glycerol nanodroplets and a cross-linking agent. The partial polymerization of the glycerol led to the formation of sponge-like nanocarriers swollen with unreacted glycerol. The control over the composition of the nanocarriers also allowed for the control of the mechanical properties of the nanocarriers. The Young's modulus of the nanocarriers was measured for different chemical compositions, and the stiffness of the nanocarriers increased with the amount of cross-linker used during the nanocarrier synthesis. Those nanocarriers were redispersed in poly(α-olefin) to create smart lubricant systems. The tribological studies of these lubricant systems in a ball-on-plates geometry showed a strong influence of the GlyNCs on the behavior of the system. Systematically, the addition of the GlyNC to the lubricant system resulted in a decrease in wear and friction at the tribological contact. In the presence of this lubricant additive, we observed up to 58% reduction in friction and up to 65% in wear compared to the pure lubricant. Ultimately, these results showed the combined effect generated by the release of glycerol and the presence of nano-objects in the tribological contact, which led to the control of the tribological properties of the system.

4. Experimental Section

Synthesis of Glycerol Nanocapsules: Glycerol nanocapsules (GlyNCs) were prepared via inverse miniemulsion. The polar phase was composed of glycerol (6.4 g; 5.2 mL; 69.5 mmol), Milli-Q water (0.32 g; 0.32 mL; 17.8 mmol), and $CaCl_2$ (70 mg; 0.5 mmol), and was stirred at 750 rpm for 5 min. Simultaneously, the nonpolar phase was prepared by dissolving PGPR (0.64 g) in toluene (69.36 g; 80 mL; 0.868 mol). The two phases were combined and stirred for 5 min at 1000 rpm. Then, the mixture was pre-emulsified for 10 min with an Ultra-Turrax at 15 000 rpm. Finally, the pre-emulsified mixture was passed through a microfluidizer (LM10, Microfluidic corp.) equipped with an F20Y interaction chamber with channels of 75 μm at a pressure of 10 000 PSI for two cycles. After emulsification, 40 mL of the resulting miniemulsion was transferred to a round bottom flask and stirred at 750 rpm. Subsequently, a solution of TDI (1.579 g; 1.294 mL; 9.066 mmol) in toluene (5.2 g; 6.0 mL; 56.5 mmol) was added dropwise through a dropping funnel. The addition of TDI dissolved in toluene was repeated at 1, 2, and 3 h after the first addition. Finally, the mixture was allowed to react overnight at room temperature.

Purification and Transfer to PAO2: The as-prepared GlyNCs were purified by centrifugation (two cycles, 4 000 rpm; 20 min) to remove PGPR and unreacted TDI. The toluene supernatant was removed and the precipitate was redispersed in fresh toluene. After another centrifugation cycle (4000 rpm; 20 min) the precipitate was finally redispersed in cyclohexane. A known amount of GlyNCs suspended in cyclohexane was added dropwise to 5 g PAO2 in a 20 mL vial while stirring vigorously to give different loading of GlyNCs in PAO2 (5, 10, and 15 wt% GlyNCs relative to PAO2). The mixture was stirred in an open vial overnight to evaporate cyclohexane and obtain a suspension of GlyNCs in PAO2.

Tribological Measurements: The tribological measurements were performed by using a ball-on-three-plates geometry attached to a rheometer (TA Discovery HR3). The stainless-steel plates were polished manually before the testing. The stainless-steel balls were used as received. A volume of 0.3 mL oil containing different loading of GlyNCs was added to the ball-on-three plates geometry, and the CoF was measured as the sliding speed of the steel-ball was ramped up from 0 to 135 mm s^{-1} followed by a ramp down from 135 to 0 mm s^{-1}. This cycle was repeated either 5 or 25 times.

Quantification of Released Glycerol: After the tribological measurement, the ball-on-three-plates geometry was rinsed with 15 mL cyclohexane to collect the suspension of GlyNCs in PAO2 entirely. Subsequently,

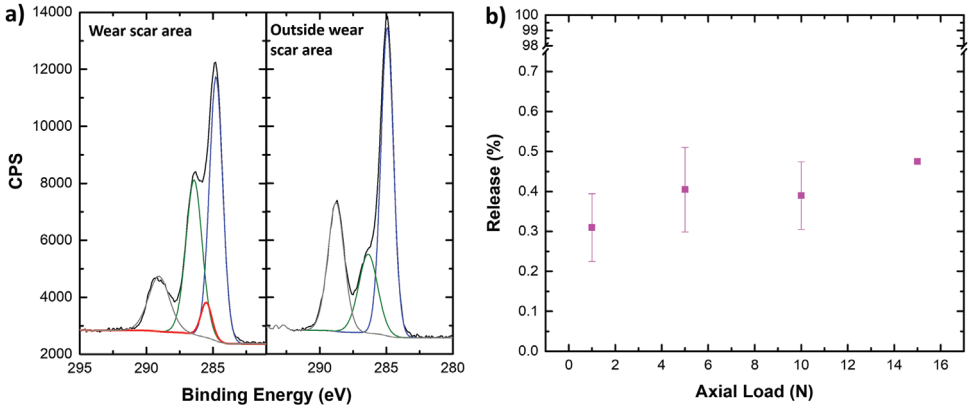

Figure 6. a) EDX measurement of metal surface after tribological measurement at the wear scar area (left) and outside the wear scar area (blue: C–C; red: C–N; green: C–O; grey: O–C═O). b) Release of glycerol into the surrounding PAO after 25 cycles at different axial loads.

the mixture was filtered through a 250 nm syringe filter to remove GlyNCs and obtain a clear liquid. The glycerol was extracted from PAO2/cyclohexane after the addition of 15 mL acetonitrile:water mixture (95:5).

After the separation of the two phases, the acetonitrile:water mixture was recovered. The concentration of glycerol in the acetonitrile:water mixture was quantified using a Hewlett Packard series 1100 HPLC system equipped with a ERC RI-101 detector, using a polar Macherey-Nagel $NH(CH_3)_2$ column (250/4.6/5 μm).

Characterization Methods: AFM measurements were performed with a JPK3 nanowizard AFM equipped with Olympus microcantilevers with a resonance frequency of 70 kHz and a spring constant of 2 N m^{-1}. To determine the Young's modulus, the substrate surface was scanned in quantitative imaging mode with an applied force of 5 nN.

TEM was performed with a JEOL 1400 electron microscope and scanning electron measurements with a 1530 Gemini LEO (Zeiss). Dynamic light scattering measurements were performed using a Malvern Zetasizer Nano-S90. Infrared spectroscopy was realized by using a PerkinElmer Spectrum BX FT-IR system. TGA measurements were performed with a TGA3 from METTLER-TOLEDO.

Supporting Information

Supporting Information is available from the Wiley Online Library or from the author.

Acknowledgements

The authors acknowledge the financial support from Fuchs Petrolub and the Max Planck Society. The authors thank Beate Müller for HPLC measurements and Andreas Hanewald for tribological measurements.

Open Access funding enabled and organized by Projekt DEAL

Conflict of Interest

The authors declare no conflict of interest.

Data Availability Statement

The data that support the findings of this study are available from the corresponding author upon reasonable request.

Keywords

friction, glycerol, lubrication, nanocarriers, wear

Received: November 1, 2021
Revised: December 7, 2021
Published online:

[1] K. Holmberg, P. Andersson, N.-O. Nylund, K. Mäkelä, A. Erdemir, *Tribol. Int.* **2014**, *78*, 94.
[2] K. Holmberg, A. Erdemir, *Friction* **2017**, *5*, 263.
[3] J. L. Mansot, Y. Bercion, L. Romana, J. M. Martin, *Braz. J. Phys.* **2008**, *39*, 186.
[4] R. Stribeck, *Die Wesentlichen Eigenschaften der Gleit- und Rollenlager*, Springer, New York **1903**.
[5] H. Spikes, *Tribol. Lett.* **2015**, *60*, 5.
[6] B. M. Fry, G. Moody, H. A. Spikes, J. S. S. Wong, *Langmuir* **2020**, *36*, 1147.
[7] I. Minami, *Appl. Sci.* **2017**, *7*, 445.
[8] Y. Long, M.-I. De Barros Bouchet, T. Lubrecht, T. Onodera, J. M. Martin, *Sci. Rep.* **2019**, *9*, 6286.
[9] L. Joly-Pottuz, J. M. Martin, M. I. De Barros Bouchet, M. Belin, *Tribol. Lett.* **2008**, *34*, 21.
[10] Y. Shi, I. Minami, M. Grahn, M. Björling, R. Larsson, *Tribol. Int.* **2014**, *69*, 39.
[11] W. Wang, B. Shen, Y. Li, Q. Ni, L. Zhou, F. Du, *Sci. Prog.* **2021**, *104*, 3685.
[12] Y. Y. Wu, W. C. Tsui, T. C. Liu, *Wear* **2007**, *262*, 819.
[13] J. Padgurskas, R. Rukuiža, R. Kreivaitis, S. J. Asadauskas, D. Bražinskienė, *Tribol.-Mater., Surf. Interfaces* **2009**, *3*, 97.
[14] J. Padgurskas, R. Rukuiza, I. Prosyčevas, R. Kreivaitis, *Tribol. Int.* **2013**, *60*, 224.
[15] Z. Tang, S. Li, *Curr. Opin. Solid State Mater. Sci.* **2014**, *18*, 119.
[16] I. Lahouij, E. W. Bucholz, B. Vacher, S. B. Sinnott, J. M. Martin, F. Dassenoy, *Nanotechnology* **2012**, *23*, 375701.
[17] W. Dai, B. Kheireddin, H. Gao, H. Liang, *Tribol. Int.* **2016**, *102*, 88.
[18] C. Weder, *J. Mater. Chem.* **2011**, *21*, 8235.
[19] M. S. Alkanawati, F. R. Wurm, H. Thérien-Aubin, K. Landfester, *Macromol. Mater. Eng.* **2018**, *303*, 1700505.
[20] N. Jagielski, S. Sharma, V. Hombach, V. Mailänder, V. Rasche, K. Landfester, *Macromol. Chem. Phys.* **2007**, *208*, 2229.
[21] C. Herrmann, D. Crespy, K. Landfester, *Colloid Polym. Sci.* **2011**, *289*, 1111.
[22] P. C. Mishra, S. Mukherjee, S. K. Nayak, A. Panda, *Int. Nano Lett.* **2014**, *4*, 109.

